MDPI

Article

Nanostructures and Thin Films of Poly(Ethylene Glycol)-Based Surfactants and Polystyrene Nanocolloid Particles on Mica: An Atomic Force Microscopy Study

John Walker [1], Andrew B. Schofield [2] and Vasileios Koutsos [1,*]

1   School of Engineering, Institute for Materials and Processes, The University of Edinburgh, Robert Stevenson Road, Edinburgh EH9 3FB, UK
2   SUPA, School of Physics and Astronomy, The University of Edinburgh, Edinburgh EH9 3FD, UK; a.b.schofield@ed.ac.uk
*   Correspondence: vasileios.koutsos@ed.ac.uk; Tel.: +44-(0)131-6508704

Abstract: We studied the nanostructures and ultrathin films resulting from the deposition and adsorption of polystyrene nanocolloidal particles and methoxy poly(ethylene glycol) methacrylate surfactants on mica surfaces from mixed suspensions in water. The samples were prepared by droplet evaporation and dip coating and imaged with atomic force microscopy. Topography and phase imaging revealed a significant richness in morphological features of the deposited/adsorbed films. We observed uniform ultrathin films and extended islands of the surfactant oligomers indicating their self-assembly in monolayers and multilayers, while the polystyrene nanocolloids were embedded within the surfactant structures. Droplet evaporation resulted in the migration of particles towards the edges of the droplet leaving an intricate network of imprints within the surfactant film. Dip coating induced the formation of extended nanocolloid clusters with colloidal crystalline structuring.

Keywords: nanocolloids; nanoparticles; nanostructures; monolayers; polymers; surfaces; thin films; mica; poly(ethylene-glycol); atomic force microscopy

1. Introduction

The self-assembly of polymers on surfaces has emerged as an elegant and inexpensive method to form nanostructures and thin films on surfaces for various applications, from functional devices [1] and nanophotonics [2] to smart nanostructured materials [3] and biomedicine [4]. Various polymer architectures have been employed including homopolymers [5], block-copolymers [6–8], random copolymers [9,10], hyperbranched polymers [11], and star polymers [12,13]. One area that is still relatively unexplored is the self-assembly of polymeric colloidal [14,15] and in particular nanocolloidal particles [16] on surfaces and the formation of associated nanostructures and thin films. This has the potential to achieve nanostructures and nanopatterns for advanced products such as high-density, defect-free data storage devices, sensors, and biochips made for a substantially lower cost than at the present and using more environmentally friendly materials and processes (suspensions of particles in water) [17–20]. In order for these colloidal particles to maintain their dispersion in a liquid suspension and not sediment out by flocculation, they must have repulsive interactions to counteract the ubiquitous attractive van der Waals forces. Colloidal particles are stabilized against this attraction either by electrostatic repulsion from surface charges [21] or with steric repulsions originating from anchored polymers or surfactants [22]. While an electrostatic interaction provides the basis of colloidal stability [23,24] by repulsion between like surface charges, it is limited because it can be used only with polar liquid mediums and it is susceptible to flocculations with extremes in pH, salt concentration, and temperature. Surfactant-based colloidal particles can be produced to provide the necessary interparticle repulsive forces in either polar or apolar mediums depending on the particular

application such as targeted drug delivery [25,26] and smart biosensors based on selective surfactant films [27]. One such surfactant is methoxy poly(ethylene glycol) methacrylate (MeOPEGMA). It consists mainly of poly(ethylene glycol) (PEG) or poly(ethylene oxide) (PEO); both terms signify the same chemical, but historically PEG has tended to refer to oligomers and polymers with a molecular mass below 20,000 g/mol and PEO to polymers with a molecular mass above 20,000 g/mol. PEG is widely used as a stabilizing agent in colloid water suspensions due to its water-solubility and its low toxicity, which make it an ideal candidate for biomedical applications [28]. Functionalisation of a colloidal surface by PEG can be achieved by combining the PEG with a suitable co-monomer which attaches to the colloidal surface, anchoring the PEG chain and thus creating a polymeric layer of steric repulsion.

The advent of scanning probe microscopy (SPM) techniques such as atomic force microscopy (AFM) has given us the ability to image and manipulate nanometre-sized particles. Apart from the high-resolution topographical imaging of a material surface, AFM [29] can also provide information on the physical properties of the material under investigation in the form of phase information [30,31] due to its direct interaction with the surface at the atomic level. The phase image contrast originates from the material's mechanical and adhesive properties, facilitating an indirect distinction between different materials/chemical species on the surface of a sample that would otherwise be undetected using topography imaging alone.

In this work, suspensions of polystyrene nanocolloidal particles copolymerised with methoxy poly(ethylene glycol) methacrylate (MeOPEGMA) surfactants were used. We deposited/adsorbed the suspension material onto mica by droplet evaporation and dip coating. In both cases, nanostructures, (sub-)monolayers, and ultrathin films were formed and studied with AFM topography and phase imaging in air. We observed the formation of highly ordered crystalline structuring of the polystyrene nanocolloids and evidence of self-assembled ultrathin films of the surfactant which originated from the nanocolloidal suspension as suspended excess material. To the best of our knowledge this is the first time that such a system has been investigated and the results we present are of an exploratory nature.

2. Experimental

The colloidal particles are made from the polymerisation of styrene molecules with a non-ionic co-monomer/stabilizer, methoxy poly(ethylene glycol) methacrylate (MeOPEGMA), in a process outlined by Ottewill et al. [32]. The MeOPEGMA polymer consists of a 2000 g/mol molecular weight PEG terminated on one end with a methoxy group. On the other end is a methyl methacrylate group which co-polymerises with the styrene and chemically links the PEG stabilizer to the particles. This results in the formation of a colloid particle with a polystyrene core and PEG polymer on its surface, which provides steric repulsion against aggregation/flocculation (PS-PEG). A 1 litre, 3-necked round-bottom flask was taken and into the 3 inlets were placed a water-cooled condenser, a nitrogen gas source, and a stirrer with a PTFE blade which was rotated at 350 rpm. The flask was placed in an oil bath which was kept at 60 °C to maintain temperature equilibrium. Into the flask were poured 475 mL of distilled water, 40.04 g (0.77 mol/dm^3) of distilled styrene, and 6.82 g of a 60% MeOPEGMA solution in water (4.1×10^{-3} mol/dm^3), which had been obtained from the Ottewill laboratory. This mixture was stirred for 20 min to allow it to come to temperature equilibrium with the oil bath. Whilst this was happening, in a separate vial the initiator solution of 0.098 g (1.12×10^{-3} mol/dm^3) of ascorbic acid, 0.22 g (3.56×10^{-3} mol/dm^3) of a 27.5% solution of hydrogen peroxide, and 22.1 g of distilled water was mixed. Once the 20 min equilibrium time had elapsed the initiator solution was added to the flask and the chemical reaction started and it was allowed to run for 6 h. The final latex particles were cleaned by centrifugation and resuspension in clean, distilled water. This process was repeated several times. The average particle diameter was measured to be 41 ± 10 nm by dynamic light scattering (DLS).

The samples for imaging were prepared in two different manners: droplet evaporation and dip coating. Mica sheets (Fisher), pre-cut to 11 mm squares, were freshly cleaved using

a scalpel along the lateral plane of the sheet inside a fume cupboard to minimise airborne pollutants from contaminating the surface. The colloidal suspensions were agitated for 30 s to ensure the minimisation of any sedimentation that may have occurred. Droplet samples were created by applying 0.16 mL of the suspension using a pipette onto the freshly cleaved mica surface. The liquid droplet completely covered the mica surface and its contact line was 'pinned' onto the mica edge. Subsequently, the sample was placed into a drying box at room temperature and pressure, in an effort to avoid heterogeneous particles from contaminating the sample. These were left until the droplet had visibly evaporated, after which the sample was placed in a glass covered Petri dish and moved into an oven at 60 °C for 1 h to ensure that any residual suspension liquid had evaporated. The dip-coated samples were prepared by submersion of the freshly-cleaved mica into a vial of the colloidal suspension in the upright position and leaving it for a predetermined incubation time. The sample was then removed and rinsed gently with deionised water followed by drying from a nitrogen jet. The sample was then placed in a glass covered Petri dish and moved into an oven at 60 °C for 1 h to ensure complete drying. If the samples were not imaged immediately after preparation, they were sealed with parafilm until imaging.

Imaging was performed using a molecular imaging PicoSPM AFM (Agilent Technologies, Santa Clara, CA, USA) operating in tapping mode (intermediate contact with the sample) using MikroMasch tips with a nominal spring constant and resonant frequency of 40 N/m and 170 kHz, respectively. The nominal tip radius was quoted as 10 nm. We operated in a light-tapping mode, where the contact amplitude approached the free oscillation amplitude of the cantilever, to minimise tip–sample interaction forces. The cantilevers were oscillated at 5% below their natural resonance frequency. For post-processing of the AFM images, the scanning probe image processor (SPIP, version 5.1.0, Image Metrology) was used. All images presented are representative of the corresponding preparation protocol and were post-processed by simple flattening alone, unless otherwise stated.

3. Results

Droplet evaporation: On imaging a droplet-prepared sample near its centre, we were presented with a topography of islands of various sizes with fractal-like edges, surrounded by an interconnected series of channels (Figure 1). The phase image shows a very high contrast between the islands and the surrounding network, indicating that there is a difference in the mechanical/adhesive properties between the two, i.e., indicating a different material. A height profile of the surface (Figure 1d) reveals a uniform island thickness of approximately 13 nm. Figure 1 shows typical AFM data from a scan area towards the centre of the sample. Moving towards the periphery of the sample, we start to observe topographical changes.

In Figure 2, we can see that the topography shows the existence of particles towards the top of the scan image. We also observe the same network of interconnected channels previously observed in Figure 1. The middle of the sample exhibits some unusual trail lines, which are clearly present on the phase image. The depth of these lines is approximately 13 nm. Towards the bottom of the topography image we see some isolated holes. The width of the isolated holes and trail lines are in the range of 40 nm.

Dip coating—incubation time 1 h: Figure 3 shows a typical example of an AFM image for a dip-coated sample for an incubation time of 1 h. We observe the presence of numerous clusters of the particles, with varying heights across the surface. We also present a selection of profiles taken across the topography image giving an indication that their heights have some preferred values: the taller clusters are approximately twice the height of the lower clusters. This is clearly demonstrated by frequency histograms of the z-heights (Figure 4) obtained by grain analysis of the cluster formations. It shows that the maximal z-height ranges have peaks at 30 nm and 60–80 nm. The area coverage has a peak value of approximately 10^5 nm^2.
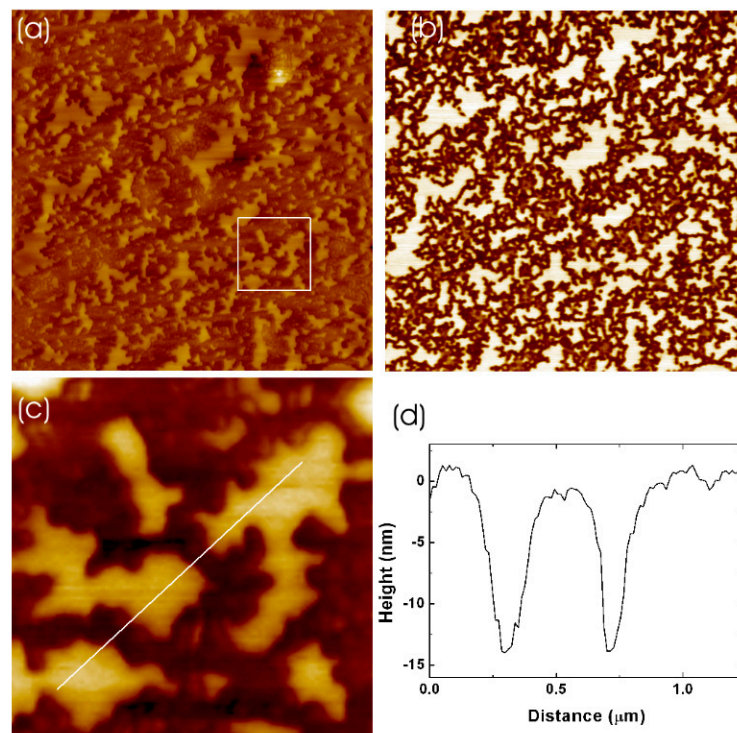
Figure 1. (**a**) 6.6 × 6.6 μm² AFM topography scan of the droplet-prepared sample (z-height scale ≈ 50 nm) with (**b**) associated phase image (voltage range 4.87 V), and (**c**) magnified section with (**d**) height profile.
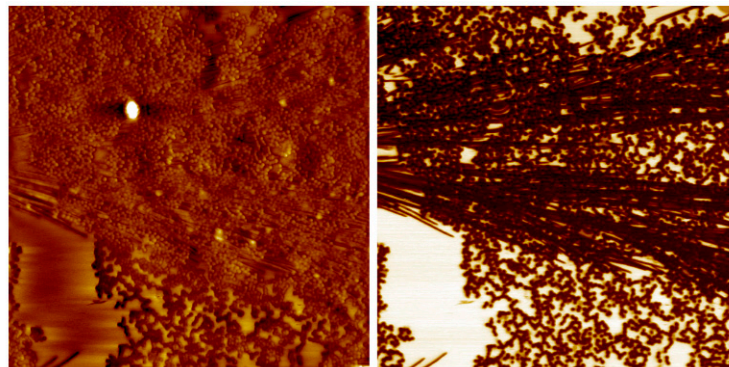

Figure 2. 6.6 × 6.6 μm² AFM topography scan of the droplet-prepared sample (**left**) with its corresponding phase image (**right**) (z-height scale ≈ 70 nm and phase voltage scale ≈ 5.2 V).

Dip coating—incubation time 72 h: Increasing the submersion time to 72 h resulted in clearly visible regular nanocolloid arrangements on the mica substrate of various lateral sizes (Figure 5). We can also observe that the surrounding areas of the particle clusters have an extended border of uniform height. This layer has been measured to be approximately 12 nm thick (Figure 6) and can be found surrounding all particle adsorption sites. The phase image suggests that there is a distinct difference between the physical properties of this plateau layer and the underlying substrate. The structuring of the particles has been observed to be highly crystalline (Figure 6c). The particles are in a close-packed hexagonal arrangement leading to very well ordered structure, as indicated by fast Fourier transform (FFT). A characteristic length of 57 nm between the particles was evaluated from the FFT graph.
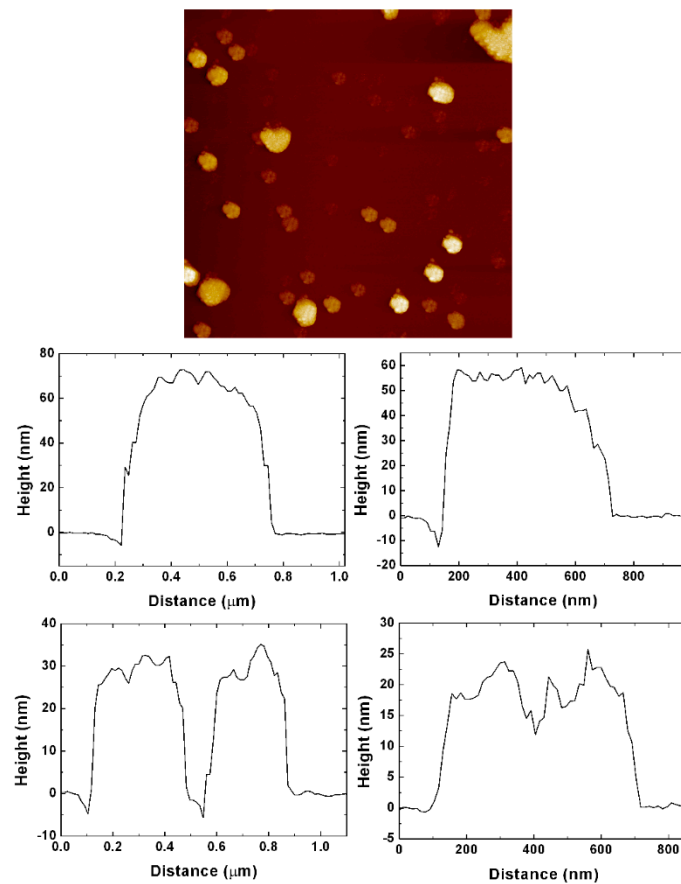
Figure 3. $6.6 \times 6.6\ \mu m^2$ AFM topography scan of the 1 h dip-coated sample (**top**) (z-height scale ≈ 80 nm) with representative height profiles of several colloidal clusters showing their relative height to the surrounding surface (**bottom**).
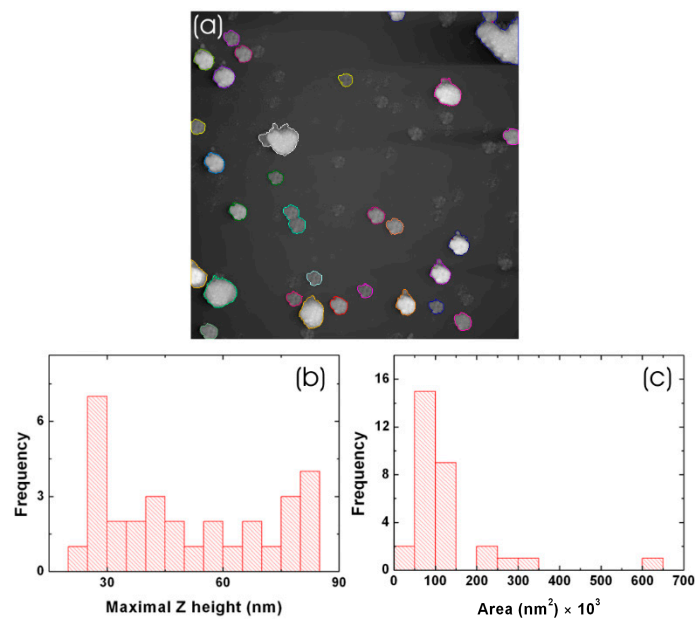

Figure 4. (**a**) Grain analysis of the $6.6 \times 6.6\ \mu m^2$ topography scan of the sample submerged for 1 h in PS–PEG. (**b**) Maximal z-height distribution relative to the surrounding surface. (**c**) Cluster area coverage distribution.
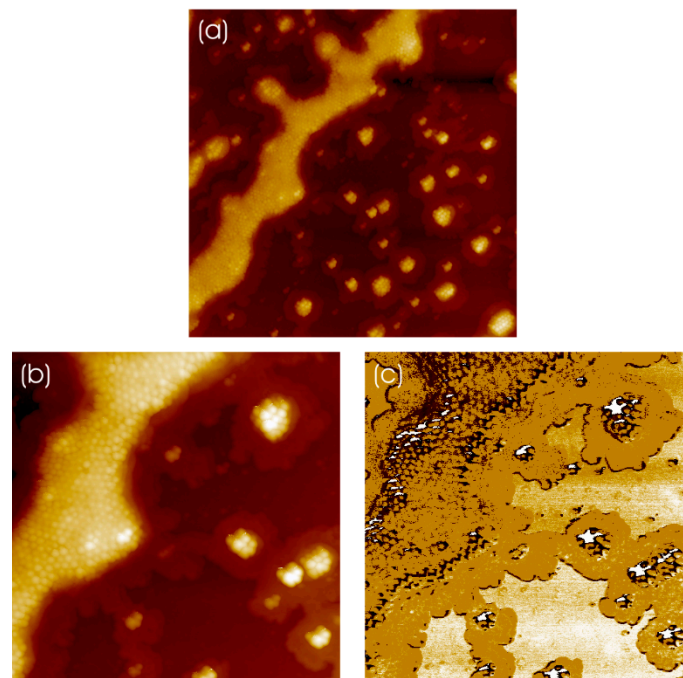
Figure 5. (**a**) 6.6 × 6.6 μm² AFM topography scan; (**b**) 3 × 3 μm² zoom scan and (**c**) its corresponding phase image showing high contrast for a sample submerged for 72 h in the suspension (z-height scale ≈ 100 nm for both topography scans, phase voltage scale ≈ 4.7 V).
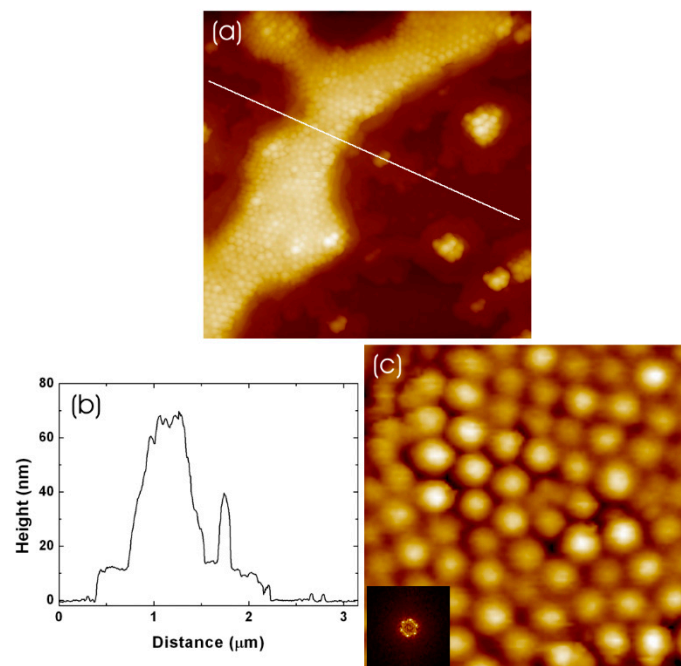

Figure 6. (**a**) 3 × 3 μm² AFM topography scan (z-height scale ≈ 100 nm); (**b**) height profile (indicated by white line on image) showing a relative height of approx. 70 nm for the large structure, approx. 40 nm for a small isolated cluster, and a surrounding plateau layer of approx. 12 nm. (**c**) Zoom of larger structure (image sharpened) showing hexagonal crystalline structuring of the particles along with (insert) its 2D FFT.

Dip coating—incubation time 240 h: After a submersion time of 10 days, scattered protrusions across the topography image were observed (Figure 7). Height profiles of the protrusions relative to the surrounding surface give a range of elevations. Grain analysis

(Figure 8) of the topography images shows that there are well-defined peaks in the relative z-heights of the protrusions at approximately 15, 25, 40, and 70 nm.
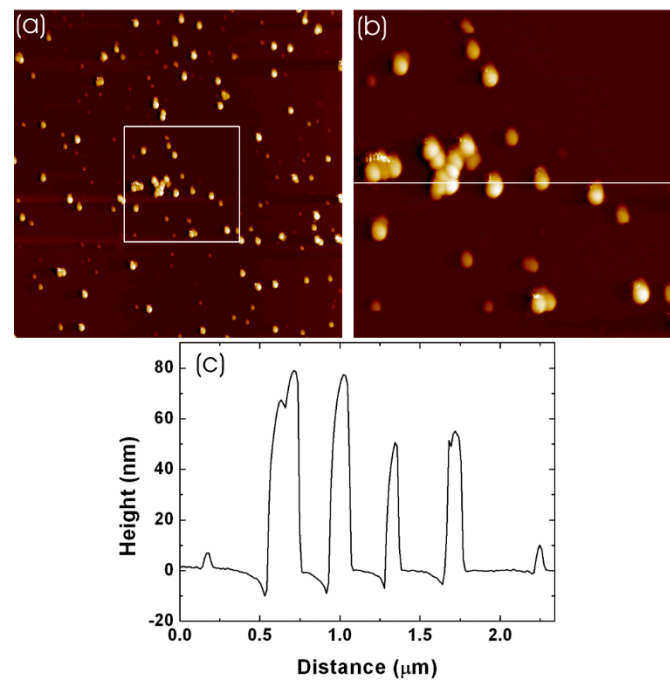

Figure 7. (**a**) 6.6×6.6 μm^2 AFM topography scan of the sample submerged for 240 h in the suspension (z-height scale $\approx$ 80 nm). (**b**) Zoom section and (**c**) corresponding height profile (indicated by white line on image).
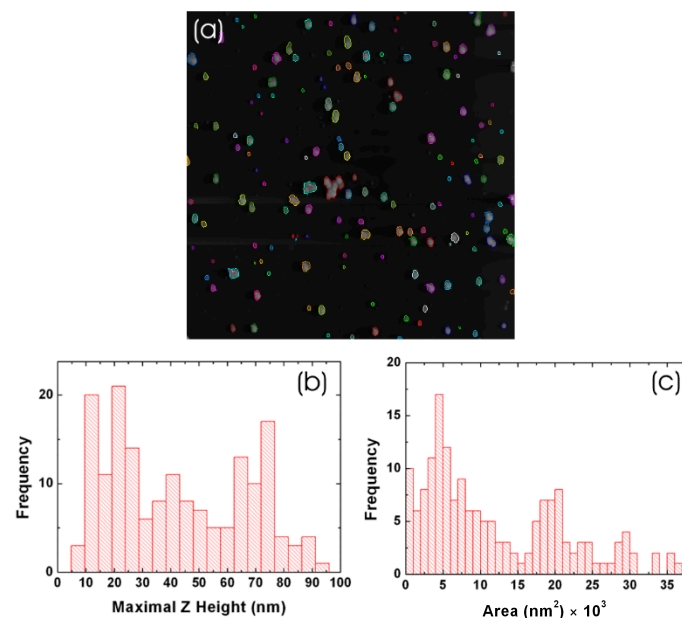

Figure 8. (**a**) Grain analysis of the 6.6×6.6 μm^2 AFM topography scan of the sample submerged for 240 h in the suspension; (**b**) z-height frequency histogram relative to the surrounding surface and (**c**) area coverage frequency histogram of protrusions.

The area coverage of the protrusions shows peaks at 5×10^3, 19×10^3, and 29×10^3 nm^2. As we would have expected, increased submersion times create higher coverage of material on this sample than seen in the 72 h dip-coating experiments. We surmise that some sort of film layer has formed on the surface of the substrate of the 240 h samples. To investigate further, the tip was raised and the AFM reconfigured for contact mode. The set-point voltage

to determine the tip contact force was raised to provide a sufficiently high enough cantilever tip-point force on the surface of the sample that would start to penetrate the film layer. The tip then scanned a square raster of approx. 1×1 μm^2 for 30 min that would effectively "dig" a hole into the surface through the film layer. The tip was then withdrawn and a tapping mode scan carried out over 4×4 μm^2 to image the dig site. As is shown in Figure 9, the dig area is clearly marked and appears to have material built up on either side. The hole is quite clean and well defined. Measurements (Figure 9d) determined the depth of the hole to be approximately 32 nm over the majority of its area. The material to the sides varies considerably in height, spanning 100–300 nm. In contrast, the material further away from the hole that was present before the digging is approximately 70 nm in height (relative to the bottom of the dig site), which is in agreement with the larger protrusions observed in Figure 7. It is interesting to note that the phase information in Figure 9 suggests that the film may be even thicker than what we dug out, as there is no contrast and thus little discernable difference in the physical properties between the surface and the bottom of the dig site, indicating the same material.
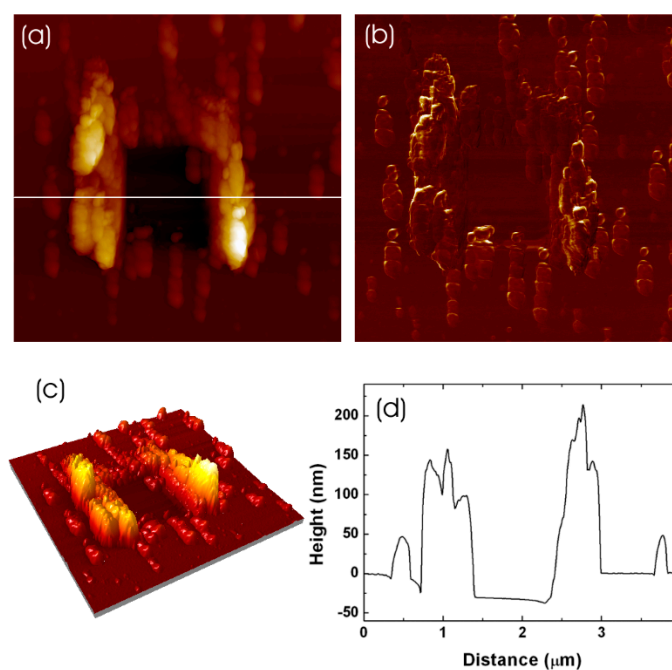

Figure 9. (**a**) 4×4 μm^2 AFM topography scan of dig site on 240 h submersion sample; (**b**) phase image; (**c**) 3D rendering of the topography and (**d**) height profile of the dig site as indicated by white line on the topography image (z-height scale $\approx$ 300 nm, phase voltage scale $\approx$ 4.6 V).

4. Discussion

Our observations (Figure 1) suggest that a uniform ultrathin film of the excess PEG-based surfactant in the colloidal suspension was formed on the mica surface during the droplet evaporation. The surfactant islands' borders form an intricate pattern of circular domains of the size of the nanocolloidal particles. It seems that both PS-PEG nanocolloids and PEG-based surfactant molecules were initially deposited on the surface but upon the slow evaporation of the droplet the subsequent convection current flows within the droplet induced desorption and redeposition of the particles towards the periphery of the sample (Figure 2). This is aided by the steric repulsion that exists between the surfactant-coated mica substrate and the PS-PEG nanocolloids. Additional evidence for this hypothesis comes from the trail lines appearing towards the perimeter of the sample (Figure 2). These lines could be caused by the PS-PEG particle being dragged as opposed to lifted due to the thinning of the droplet's contact line as it nears complete evaporation of the liquid. The existence of particles at the perimeter also suggests mass transport within the droplet.

The initiation of convection flows within the droplet as it began to evaporate caused the nanocolloids that were initially deposited on the sample surface to be lifted or dragged along to the extremities. The mechanism of movement of suspended material towards the periphery is well documented in other experimental work as the "coffee stain effect" [33], where a pinned droplet will stream liquid towards the perimeter in order to replace the evaporating liquid carrying within it any particulates in suspension [34].

The apparent thickness of the thin film is approximately 13 nm, which is compatible with a dense self-assembled monolayer (SAM) of the MeOPEGMA oligomer that has a contour length of about 16 nm [35]. We note that we have imaged in ambient conditions; due to the humidity in the environment and to the fact that both mica and PEG have a high affinity for water, there is the opportunity for the PEG SAM to be swollen [12]. The MeOPEGMA oligomer terminates at one end with a methyl methacrylate group which is hydrophobic while PEG is hydrophilic. If we consider that the PEG component of the surfactant has a very high affinity for water then there would be no reason for it to adsorb onto the surface for any of the submersion samples [36,37]; the methacrylate termination group, however, will be in a bad solvent when in water, and so will prefer to align to the mica surface [38]. If this adsorption configuration occurred at a high enough adsorption density it would have the effect of creating a self-assembled monolayer of surfactant chains in a brush regime. We note that when the samples are removed from the water suspension the hydrophilic mica retains an ultrathin layer of water and could attract the PEG [39,40], changing the orientation of MeOPEGMA.

In the dip-coated samples, we have also observed a layer of approx. 12 nm surrounding the nanocolloid structures (Figure 6). In these samples we also see some evidence of slight steps in the surrounding layer edge which could come from capillary forces as the liquid around the nanocolloid structure evaporates. We note that there is an evaporation process of the remaining ultrathin water domains at the micro/nanoscale for the dip-coated samples even if most of the liquid has been dried by nitrogen injection [12]. The surfactants exposed at the edge of the plateau will subside and tilt in some form creating small nanometre-size steps. Parallel layering to the sample substrate cannot be excluded.

The clustering observed in the 1 h submersion samples (Figure 3) showed some interesting configurations. Grain analysis showed that the z-heights relative to the surrounding surface had quite well-defined peaks at 30 and 70 nm, suggesting that there is evidence of bilayering occurring in the cluster structure. This is reinforced by the area histogram which has a very strong peak in the region of the $\approx 90 \times 10^3$ nm^2, indicating that there seems to be a preferred size for the area occupied by the cluster. The (≈ 10 nm) lower than expected height values could be the result of a thin film of surfactant having already formed on the mica substrate (approx. 12–13 nm). Thus, the height peaks compare well for a particle monolayer and bilayer since the particle size of the PS-PEG particles is ≈ 41 nm.

The 240 h incubation samples were submerged for the longest time in this study and they had the highest material coverage of all the samples under investigation, as shown by the digging experiment (Figure 9). The depth of the dig site (32 nm) indicates that there is a bilayer, if not multilayer, of the surfactant present on the mica substrate. The hydrophilic nature of the PEG combined with the hydrophobic methyl methacrylate termination would facilitate such multilayer lamellar structuring. This configuration could explain the range of protrusion sizes for these samples.

Further evidence for the multilayer surfactant formation comes from the grain analysis (Figure 8). The z-height histograms indicate reoccurring peaks relative to the surrounding surface at 15 nm, 25 nm, 40 nm, and 70 nm. Peaks also appear on the area measurements at 5×10^3, 19×10^3, and 29×10^3 nm^2. This multimodal distribution suggests that there are regular separations in the z-heights, the differences are in the region of 15–30 nm which would fit well with our proposed lamellar structuring of the surfactant. If this is the case, then particles have become trapped on different layers of the surfactant; the multimodal distribution in the area measurements promotes this idea; particles at different,

but well defined, depths will protrude through to the top layer creating a series of defined protrusions on the surface.

The FFT of the particle structures for the 72 h incubation time sample showed highly ordered crystalline structuring of the PS-PEG particles (Figure 6). It revealed that the characteristic length between the particles was 57 nm. The larger than expected length could be due to the presence of the dry surfactant layer between them. The self-assembled crystalline structures were formed due to capillary/meniscus forces towards the final steps of the drying/evaporation; at this point the necessary interparticle forces required to draw the particles closely together were generated [41,42]. A meniscus must exist between the particles of the suspension liquid in order to generate the capillary forces when the particles are still partially submerged in liquid at this point.

5. Conclusions

We found that the PS-PEG colloidal suspension containing an excess of PEG-based surfactant molecules produced mixed monolayers, (sub-)monolayers, and ultrathin films on the mica surface. Our AFM study indicates that the PEG-based surfactant organised into self-assembled monolayers and multilayer ultrathin films. Flow currents during the droplet evaporation led to the desorption and redeposition of PS-PEG colloidal nanoparticles into the periphery of the sample, leaving the formation of an imprint of the particle deposition towards the centre of the samples and thus creating a 'fingerprint' of the nanocolloid initial structuring. The dip-coated samples showed a rich range of nanostructures including highly ordered domains of the PS-PEG particles at low incubation times and particles embedded in a multilayer surfactant ultrathin film at higher incubation times. To the best of our knowledge this system has not been studied before and our AFM study indicates the presence of very interesting nanostructures and nanopatterns which could be relevant for many applications.

Author Contributions: Conceptualization, V.K. and J.W.; methodology, V.K. and J.W.; software, J.W.; validation, J.W., V.K. and A.B.S.; formal analysis, J.W.; investigation, J.W.; resources, V.K. and A.B.S.; data curation, J.W.; writing—original draft preparation, J.W.; writing—review and editing, J.W., V.K. and A.B.S.; visualization, J.W.; supervision, V.K.; project administration, V.K.; funding acquisition, J.W. and V.K. All authors have read and agreed to the published version of the manuscript.

Institutional Review Board Statement: Not applicable.

Informed Consent Statement: Not applicable.

Data Availability Statement: Data available upon request.

Conflicts of Interest: The authors declare that they have no conflict of interest.

References

1. Pinto-Gómez, C.; Pérez-Murano, F.; Bausells, J.; Villanueva, L.G.; Fernández-Regúlez, M. Directed Self-Assembly of Block Copolymers for the Fabrication of Functional Devices. *Polymers* **2020**, *12*, 2432. [CrossRef] [PubMed]
2. Kulkarni, A.A.; Doerk, G.S. Thin film block copolymer self-assembly for nanophotonics. *Nanotechnology* **2022**, *33*, 292001. [CrossRef]
3. Kim, J.H.; Jin, H.M.; Yang, G.G.; Han, K.H.; Yun, T.; Shin, J.Y.; Jeong, S.-J.; Kim, S.O. Smart Nanostructured Materials based on Self-Assembly of Block Copolymers. *Adv. Funct. Mater.* **2020**, *30*, 1902049. [CrossRef]
4. Li, J.; Wang, J.; Chen, L.; Dong, Y.; Chen, H.; Nie, G.; Li, F. Self-assembly of DNA molecules at bio-interfaces and their emerging applications for biomedicines. *Nano Res.* **2023**. [CrossRef]
5. Glynos, E.; Chremos, A.; Camp, P.J.; Koutsos, V. Surface Nanopatterning Using the Self-Assembly of Linear Polymers on Surfaces after Solvent Evaporation. *Nanomanuf. Metrol.* **2022**, *5*, 297–309. [CrossRef]

6. Cummins, C.; Lundy, R.; Walsh, J.J.; Ponsinet, V.; Fleury, G.; Morris, M.A. Enabling future nanomanufacturing through block copolymer self-assembly: A review. *Nano Today* **2020**, *35*, 100936. [CrossRef]

7. Karayianni, M.; Pispas, S. Block copolymer solution self-assembly: Recent advances, emerging trends, and applications. *J. Polym. Sci.* **2021**, *59*, 1874–1898. [CrossRef]

8. Brassat, K.; Lindner, J.K.N. Nanoscale Block Copolymer Self-Assembly and Microscale Polymer Film Dewetting: Progress in Understanding the Role of Interfacial Energies in the Formation of Hierarchical Nanostructures. *Adv. Mater. Interfaces* **2020**, *7*, 1901565. [CrossRef]

9. McClements, J.; Shaver, M.P.; Sefiane, K.; Koutsos, V. Morphology of Poly(styrene-co-butadiene) Random Copolymer Thin Films and Nanostructures on a Graphite Surface. *Langmuir* **2018**, *34*, 7784–7796. [CrossRef]

10. McClements, J.; Buffone, C.; Shaver, M.P.; Sefiane, K.; Koutsos, V. Poly(styrene-co-butadiene) random copolymer thin films and nanostructures on a mica surface: Morphology and contact angles of nanodroplets. *Soft Matter* **2017**, *13*, 6152–6166. [CrossRef]

11. Zhou, Y.; Huang, W.; Liu, J.; Zhu, X.; Yan, D. Self-Assembly of Hyperbranched Polymers and Its Biomedical Applications. *Adv. Mater.* **2010**, *22*, 4567–4590. [CrossRef] [PubMed]

12. Glynos, E.; Chremos, A.; Petekidis, G.; Camp, P.J.; Koutsos, V. Polymer-like to Soft Colloid-like Behavior of Regular Star Polymers Adsorbed on Surfaces. *Macromolecules* **2007**, *40*, 6947–6958. [CrossRef]

13. Mendrek, B.; Oleszko-Torbus, N.; Teper, P.; Kowalczuk, A. Towards next generation polymer surfaces: Nano- and microlayers of star macromolecules and their design for applications in biology and medicine. *Prog. Polym. Sci.* **2023**, *139*, 101657. [CrossRef]

14. Zhang, J.; Sun, Z.; Yang, B. Self-assembly of photonic crystals from polymer colloids. *Curr. Opin. Colloid Interface Sci.* **2009**, *14*, 103–114. [CrossRef]

15. van Dommelen, R.; Fanzio, P.; Sasso, L. Surface self-assembly of colloidal crystals for micro- and nano-patterning. *Adv. Colloid Interface Sci.* **2018**, *251*, 97–114. [CrossRef] [PubMed]

16. MacFarlane, L.R.; Shaikh, H.; Garcia-Hernandez, J.D.; Vespa, M.; Fukui, T.; Manners, I. Functional nanoparticles through π-conjugated polymer self-assembly. *Nat. Rev. Mater.* **2021**, *6*, 7–26. [CrossRef]

17. Martin, C.P.; Blunt, M.O.; Vaujour, E.; Fahmi, A.; D'Aléo, A.; De Cola, L.; Vögtle, F.; Moriarty, P. Chapter 1 Self-Organised Nanoparticle Assemblies: A Panoply of Patterns. In *Studies in Multidisciplinarity*; Krasnogor, N., Gustafson, S., Pelta, D.A., Verdegay, J.L., Eds.; Elsevier: Amsterdam, The Netherlands, 2008; Volume 5, pp. 1–20.

18. Mutch, K.J.; Koutsos, V.; Camp, P.J. Deposition of Magnetic Colloidal Particles on Graphite and Mica Surfaces Driven by Solvent Evaporation. *Langmuir* **2006**, *22*, 5611–5616. [CrossRef] [PubMed]

19. Xia, Y.; Gates, B.; Yin, Y.; Lu, Y. Monodispersed Colloidal Spheres: Old Materials with New Applications. *Adv. Mater.* **2000**, *12*, 693–713. [CrossRef]

20. Zbonikowski, R.; Mente, P.; Bończak, B.; Paczesny, J. Adaptive 2D and Pseudo-2D Systems: Molecular, Polymeric, and Colloidal Building Blocks for Tailored Complexity. *Nanomaterials* **2023**, *13*, 855. [CrossRef]

21. Scherer, C.; Figueiredo Neto, A. Ferrofluids: Properties and Applications. *Braz. J. Phys.* **2005**, *35*, 718–727. [CrossRef]

22. Ghodbane, J.; Denoyel, R. Competitive adsorption between non-ionic polymers and surfactants on silica. *Colloids Surf. A Physicochem. Eng. Asp.* **1997**, *127*, 97–104. [CrossRef]

23. Verwey, E.J.W.; Overbeek, J.T.G. *Theory of the Stability of Lyophobic Colloids*; Elsevier Publishing Co.: New York, NY, USA; Amsterdam, The Netherlands; London, UK; Brussels, Belgium, 1948; p. 205.

24. Derjaguin, B.; Landau, L. Theory of the stability of strongly charged lyophobic sols and of the adhesion of strongly charged particles in solutions of electrolytes. *Prog. Surf. Sci.* **1993**, *43*, 30–59. [CrossRef]

25. Drummond, C.J.; Fong, C. Surfactant self-assembly objects as novel drug delivery vehicles. *Curr. Opin. Colloid Interface Sci.* **1999**, *4*, 449–456. [CrossRef]

26. Torchilin, V.P. Structure and design of polymeric surfactant-based drug delivery systems. *J. Control. Release* **2001**, *73*, 137–172. [CrossRef] [PubMed]

27. Velev, O.D.; Kaler, E.W. In Situ Assembly of Colloidal Particles into Miniaturized Biosensors. *Langmuir* **1999**, *15*, 3693–3698. [CrossRef]

28. Otsuka, H.; Nagasaki, Y.; Kataoka, K. Self-assembly of poly(ethylene glycol)-based block copolymers for biomedical applications. *Curr. Opin. Colloid Interface Sci.* **2001**, *6*, 3–10. [CrossRef]

29. Butt, H.J.; Berger, R.; Bonaccurso, E.; Chen, Y.; Wang, J. Impact of atomic force microscopy on interface and colloid science. *Adv. Colloid Interface Sci.* **2007**, *133*, 91–104. [CrossRef]

30. Schmitz, I.; Schreiner, M.; Friedbacher, G.; Grasserbauer, M. Phase imaging as an extension to tapping mode AFM for the identification of material properties on humidity-sensitive surfaces. *Appl. Surf. Sci.* **1997**, *115*, 190–198. [CrossRef]

31. Bar, G.; Thomann, Y.; Brandsch, R.; Cantow, H.J.; Whangbo, M.H. Factors Affecting the Height and Phase Images in Tapping Mode Atomic Force Microscopy. Study of Phase-Separated Polymer Blends of Poly(ethene-co-styrene) and Poly(2,6-dimethyl-1,4-phenylene oxide). *Langmuir* **1997**, *13*, 3807–3812. [CrossRef]

32. Ottewill, R.H.; Satgurunathan, R. Nonionic latices in aqueous media part 1. Preparation and characterization of polystyrene latices. *Colloid Polym. Sci.* **1987**, *265*, 845–853. [CrossRef]

33. Deegan, R.D.; Bakajin, O.; Dupont, T.F.; Huber, G.; Nagel, S.R.; Witten, T.A. Capillary flow as the cause of ring stains from dried liquid drops. *Nature* **1997**, *389*, 827–829. [CrossRef]

34. Askounis, A.; Sefiane, K.; Koutsos, V.; Shanahan, M.E.R. Structural transitions in a ring stain created at the contact line of evaporating nanosuspension sessile drops. *Phys. Rev. E* **2013**, *87*, 012301. [CrossRef] [PubMed]
35. Wang, T.; Xu, J.; Qiu, F.; Zhang, H.; Yang, Y. Force spectrum of a few chains grafted on an AFM tip: Comparison of the experiment to a self-consistent mean field theory simulation. *Polymer* **2007**, *48*, 6170–6179. [CrossRef]
36. Chai, L.; Klein, J. Role of Ion Ligands in the Attachment of Poly(ethylene oxide) to a Charged Surface. *J. Am. Chem. Soc.* **2005**, *127*, 1104–1105. [CrossRef] [PubMed]
37. Geke, M.O.; Shelden, R.A.; Caseri, W.R.; Suter, U.W. Ion Exchange of Cation-Terminated Poly(ethylene oxide) Chains on Mica Surfaces. *J. Colloid Interface Sci.* **1997**, *189*, 283–287. [CrossRef]
38. Kumaki, J.; Nishikawa, Y.; Hashimoto, T. Visualization of Single-Chain Conformations of a Synthetic Polymer with Atomic Force Microscopy. *J. Am. Chem. Soc.* **1996**, *118*, 3321–3322. [CrossRef]
39. Glynos, E.; Pispas, S.; Koutsos, V. Amphiphilic Diblock Copolymers on Mica: Formation of Flat Polymer Nanoislands and Evolution to Protruding Surface Micelles. *Macromolecules* **2008**, *41*, 4313–4320. [CrossRef]
40. Kalloudis, M.; Glynos, E.; Pispas, S.; Walker, J.; Koutsos, V. Thin Films of Poly(isoprene-b-ethylene Oxide) Diblock Copolymers on Mica: An Atomic Force Microscopy Study. *Langmuir* **2013**, *29*, 2339–2349. [CrossRef] [PubMed]
41. Kralchevsky, P.A.; Denkov, N.D. Capillary forces and structuring in layers of colloid particles. *Curr. Opin. Colloid Interface Sci.* **2001**, *6*, 383–401. [CrossRef]
42. Kralchevsky, P.A.; Nagayama, K. Capillary forces between colloidal particles. *Langmuir* **1994**, *10*, 23–36. [CrossRef]